Original Article

Assessment of aortic hemodynamics in patients with thoracoabdominal aortic aneurysm using four-dimensional magnetic resonance imaging: a cross-sectional study

Wen Zeng[1#], Jiarong Wang[2#], Chengxin Weng[2], Wanlin Peng[1], Tiehao Wang[2], Ding Yuan[2], Bin Huang[2], Jichun Zhao[2], Chunchao Xia[1], Zhenlin Li[1], Yingkun Guo[3]

[1]Department of Radiology, West China Hospital, Sichuan University, Chengdu, China; [2]Division of Vascular Surgery, Department of General Surgery, West China Hospital, Sichuan University, Chengdu, China; [3]Department of Radiology, Development and Related Diseases of Women and Children Key Laboratory of Sichuan Province, West China Second University Hospital, Sichuan University, Chengdu, China

Contributions: (I) Conception and design: Z Li, Y Guo; (II) Administrative support: J Wang, W Zeng, C Weng, D Yuan, T Wang, B Huang; (III) Provision of study materials or patients: W Zeng, W Peng, C Xia, Z Li, Y Guo; (IV) Collection and assembly of data: J Wang, W Zeng, C Weng, W Peng; (V) Data analysis and interpretation: B Huang, J Zhao, D Yuan, C Xia, Z Li, Y Guo; (VI) Manuscript writing: All authors; (VII) Final approval of manuscript: All authors.

[#]These authors contributed equally to this work.

Correspondence to: Zhenlin Li, PhD. Department of Radiology, West China Hospital, Sichuan University, No. 37 Guoxue Lane, Wuhou District, Chengdu, China. Email: HX_lizhenlin@126.com; Yingkun Guo, PhD. Department of Radiology, Development and Related Diseases of Women and Children Key Laboratory of Sichuan Province, West China Second University Hospital, Sichuan University, No. 20, Section 3, Renmin South Road, Wuhou District, Chengdu, China. Email: gykpanda@163.com.

Background: Thoracoabdominal aortic aneurysms (TAAAs) are rare but complicated aortic pathologies that can result in high morbidity and mortality. The whole-aorta hemodynamic characteristics of TAAA survivors remains unknown. This study sought to obtain a comprehensive view of flow hemodynamics of the whole aorta in patients with TAAA using four-dimensional flow (4D flow) magnetic resonance imaging (MRI).

Methods: This study included patients who had experienced TAAA or abdominal aortic aneurysm (AAA) and age- and sex-matched volunteers who had attended China Hospital from December 2021 to December 2022 in West. Patients with unstable ruptured aneurysm or other cardiovascular diseases were excluded. 4D-flow MRI that covered the whole aorta was acquired. Both planar parameters [(regurgitation fraction (RF), peak systolic velocity (V_{max}), overall wall shear stress (WSS)] and segmental parameters [pulse wave velocity (PWV) and viscous energy loss (VEL)] were generated during postprocessing. The Student's *t*-test or Mann-Whitney test was used to compare flow dynamics among the three groups.

Results: A total of 11 patients with TAAA (mean age 53.2±11.9 years; 10 males), 19 patients with AAA (mean age 58.0±11.7 years; 16 males), and 21 controls (mean age 55.4±15.0 years; 19 males) were analyzed. The patients with TAAA demonstrated a significantly higher RF and lower Vmax in the aortic arch compared to healthy controls. The whole length of the aorta in patients with TAAA was characterized by lower WSS, predominantly in the planes of pulmonary artery bifurcation and the middle infrarenal planes (all P values <0.001). As for segmental hemodynamics, compared to controls, patients with TAAA had a significantly higher PWV in the thoracic aorta (TAAA: median 11.41 m/s, IQR 9.56–14.32 m/s; control: median 7.21 m/s, IQR 5.57–7.79 m/s; P<0.001) as did those with AAA (AAA: median 8.75 m/s, IQR 7.35–10.75 m/s; control: median 7.21 m/s, IQR 5.57–7.79 m/s; P=0.024). Moreover, a greater VEL was observed in the whole aorta and abdominal aorta in patients with TAAA.

Conclusions: Patients with TAAA exhibited a stiffer aortic wall with a lower WSS and a greater VEL for the whole aorta, which was accompanied by a higher RF and lower peak velocity in the dilated portion of the aorta.

Keywords: Thoracoabdominal aortic aneurysm (TAAA); abdominal aortic aneurysm (AAA); four-dimensional flow magnetic resonance imaging (4D flow MRI); hemodynamics

Submitted Sep 17, 2023. Accepted for publication Feb 19, 2024. Published online Mar 28, 2024.
doi: 10.21037/qims-23-1321
View this article at: https://dx.doi.org/10.21037/qims-23-1321

Introduction

Thoracoabdominal aortic aneurysm (TAAA) is a challenging cardiovascular disease and is characterized by continuous dilation of the descending thoracic aorta extending into the abdominal aorta (1), which can be life-threatening if left untreated due to the related risk of rupture. The current guidelines from American College of Cardiology/American Heart Association (ACC/AHA) recommend surgical intervention of TAAA if the aortic diameter exceeds 5.5 cm or grows faster than 5 mm per year (2,3). Data from the National Cerebral and Cardiovascular Center of Japan revealed that the incidence of rupture increases with larger aortic size, rising sharply up to 18% when the diameter of aorta reaches 5.5 cm (4). However, according to data from another large database of descending thoracic or TAAAs in North America, 7% patients of these patients still experience rupture at a diameter below 5.0 cm (5). Therefore, the evaluation of patients at high risk of rupture solely based on aortic diameter remains to be completed and requires the effective ancillary assessment of other parameters.

A growing body of evidence accumulated over the past decade suggests that certain hemodynamic parameters, such as wall shear stress (WSS), are associated with an increased risk of aneurysm expansion and rupture (6-9). Although computational fluid dynamics (CFD) technology has revolutionized cardiovascular research by facilitating the detailed characterization of advanced physiological metrics in flow fields of interest, several limitations in CFD studies exist. For instance, the increasing complexity of various parameter inputs for simulating patient-specific conditions has necessitated the development of powerful computational tools, which are also needed to cope with the exponential growth of data and time-consuming postprocessing that limit the clinical use of CFD (10,11). By comparison, advanced time-resolved three-dimensional (3D) phase-contrast (PC) cardiovascular magnetic resonance (CMR), also known as four-dimensional (4D) flow magnetic resonance imaging (MRI), can capture individual-specific flow velocity and volume in blood vessels while visualizing the blood streamline flow in real time (12). Research suggests that 4D flow MRI can well depict blood flow characteristics and postoperative changes in the thoracic aortic domain (13-16), but few studies have reported the blood flow dynamics of 4D flow MRI in abdominal aortic aneurysms (AAA), much less in TAAA.

Therefore, our study aimed to compare the abnormal blood flow hemodynamics of the whole segment of aorta in patients with TAAA or AAA patients using 4D flow MRI with those of age- and sex-matched nondilated control volunteers. Flow patterns and hemodynamic parameters from planes (11 planes from the aortic root to the abdominal aortic bifurcation) and segments (thoracic, abdominal, whole aorta) were analyzed to complete a multidimensional characterization of the flow dynamics in patients with TAAA or AAA and to compare them with those of with age- and sex-matched controls. We present this article in accordance with the STROBE reporting checklist (available at https://qims.amegroups.com/article/view/10.21037/qims-23-1321/rc).

Methods

Study design

This cross-sectional study included patients with TAAA, patients with AAA, and nondilated volunteers from a prospective, nested, case-control study registered on the Chinese Clinical Trial Registry (trial registration number: ChiCTR2100054252; date: December 11, 2021).

Participants

All consecutive patients who were diagnosed with TAAA or

AAA in West China Hospital were assessed for enrollment eligibility from December 2021 to December 2022. Patients were excluded from the TAAA and AAA groups if they met any of the following criteria: (I) hemodynamically unstable ruptured TAAA or AAA; (II) contraindications to 3T MRI scanning, for example, implantation of electronic cardiac pacemaker, claustrophobia, and uncontrolled arrhythmia; (III) refusal to participate in the study; and (IV) presence of other cardiovascular diseases, including congenital heart disease, valve disease, arteritis, etc. TAAA was defined as continuous dilation (to at least 1.5 times the normal diameter) of the descending thoracic aorta extending into the abdominal aorta. The diagnosis of AAA was made if the maximum diameter of the infrarenal abdominal aorta exceeded 3.5 cm.

The control group consisted of those who participated in our study as volunteers without evidence of aortic dilation in the same time period. Individuals in the control group were matched by age and gender at a ratio of approximately 1:2. Volunteers were excluded if they had contraindications for 3T MRI scanning or they refused to sign the informed consent. The age, gender, body mass index (BMI), heart rate, hypertension, and other comorbidities were matched between each group. This study was conducted in accordance with the Declaration of Helsinki (as revised in 2013) and was approved by ethics committee of West China Hospital, Sichuan University (reference number 2021-1171). Informed consent was obtained from all individual participants.

4D flow MRI acquisition

All participants underwent CMR exams on a 3.0T CMR system (Ingenia Elition, Philips Healthcare, Netherlands) equipped with a 32-channel phased array body coil. The main scanning protocol involved the following sequences: (I) 2D time-resolved PC MRI with velocity encoding and (II) 4D flow MRI with the echo planar imaging (EPI) readout acquisition technique. The scanning field covered the whole range of the thoracic and abdominal aorta, in addition to the bilateral common iliac arteries.

First, the 2D flow MRI was scanned to determine the maximum velocity in the scanning range, with a spatial resolution of 1.2×1.2×8.0 mm^3 in 40 heart phases. 4D flow MRI was then acquired with a flip angle of 7° and an echo time (TE)/repetition time (TR) of 4.1/8.0 msec. 4D flow data with retrospective electrocardiographic (ECG) triggering were acquired in 25 heart phases during free-breathing without respiratory navigator gating. The field of was were (440–490)×(390–420)×(122–170) mm^3 in size. Acquisition spatial resolution and reconstructed spatial resolution were 2.5×2.5×2.5 mm^3 and 2.0×2.0×2.5 mm^3 in size, respectively. Three-directional velocity-encoding sensitivity (VENC) was set to 80–150 cm/second depending on the velocity in 2D PC MRI scout images.

Image processing and analysis

The 4D flow data sets were analyzed using a commercial postprocessing software, CVI 42 (Circle Cardiovascular Imaging Inc., Canada). Offset correction and phase unwrapping were used to address any phase offset aliasing and image noise for 4D flow datasets (13). The aortic wall was automatically segmented through tracking the center line using CVI42 software.

A total of 11 planes were set at the following regions of interest (ROIs) perpendicular to the vessel centerline (*Figure 1*): (I) aortic root, (II) middle of the ascending aorta, (III) brachiocephalic trunk (BCT), (IV) left common carotid artery (LCCA), (V) left subclavian artery (LSA), (VI) descending aorta at the level of pulmonary trunk bifurcation, (VII) descending aorta at the level of the heart apex or diaphragm, (VIII) celiac trunk, (IX) renal artery, (X) middle of the infrarenal segment, and (XI) aortic bifurcation. For those patients with aneurysm, the nearest ROI was taken at the level of the maximum diameter of the aneurysm.

Planar hemodynamic parameters were measured at the above 11 ROIs and involved total flow volume (TFV), regurgitation fraction (RF), peak systolic velocity (V_{max}), overall WSS, circumferential WSS (cir-WSS), and axial WSS (axi-WSS). WSS is a vector quantity that captures how complex flow can induce shear forces along the lumen circumference (cir-WSS) and along the main flow direction (axi-WSS). These parameters were calculated according to the work of Sotelo *et al.* (17). The whole length of aorta was divided into two segments: the thoracic aorta (from the aortic root to the renal artery) and abdominal aorta (from the renal artery to the aortic bifurcation). The thoracic aorta was further divided into three segments: the ascending aorta (from the aortic root to the BCT), arch (from the BCT to the LSA), and descending aorta (from the LSA to the renal artery). These segments were included in segmental hemodynamics analysis, which mainly included the following parameters: pulse wave velocity (PWV) and viscous energy loss (VEL). PWV is a parameter widely used

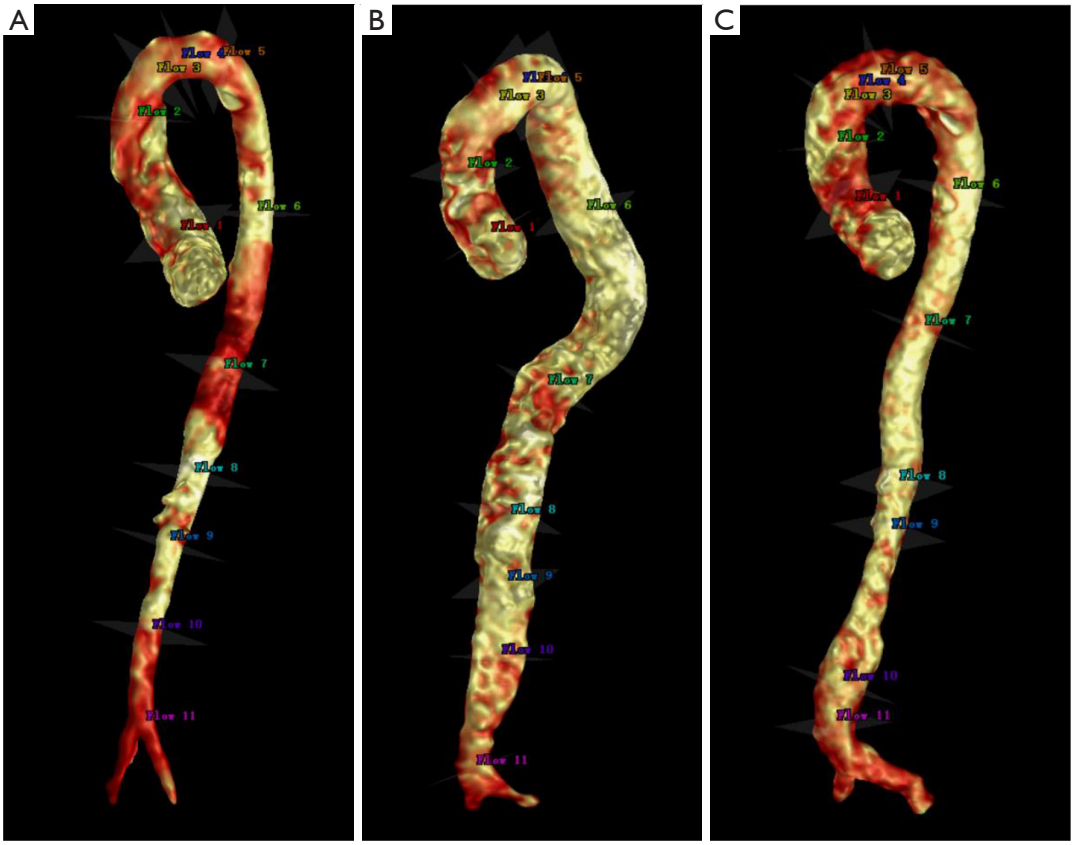

Figure 1 Postprocessing of 4D flow imaging with 11 regions of interest perpendicular to the vessel centerline among (A) age- and sex-matched controls, (B) patients with TAAA, and (C) patients with AAA. 4D, four-dimensional; TAAA, thoracoabdominal aortic aneurysm; AAA, abdominal aortic aneurysm.

to assess the arterial stiffness and consists of the speed of the arterial pressure waves traveling along the large artery of interest (18,19). VEL refers to the mechanical kinetic energy irreversibly lost (converted) to thermal energy caused by friction of the blood against the aortic wall induced by fluid viscosity and a no-slip condition (20-22). In addition, flow pattern was qualitatively evaluated as follows: vortical flow was defined as the blood flow along a curved path or the flow of a rotating mass, and helical flow was defined as the cork-screw-like flow of blood in the blood vessel. A sketch of the flow and helical flow is shown in Figure S1.

All image processing was performed by one radiologist and one vascular surgeon who were blinded to the enrollment and clinical data. In order to ensure the reliability of the measurement, two observers received training before the image postprocessing and arrived at a consensus for a standardized measuring protocol. Moreover, the interobserver variability of the hemodynamic parameters was assessed in the first 10 participants, and further agreement was reached before the data processing of all participants.

Statistical analysis

Continuous data are expressed as the mean ± standard deviation (SD) if they were normally distributed or as the median [interquartile range (IQR)] otherwise. The Shapiro-Wilk test was adopted to test the normality of the data distribution. Comparison was performed using the two-tailed unpaired *t*-test if the data were normally distributed or otherwise, with the Mann-Whitney test. The χ^2 test or Fischer exact test was adopted to compare categorical data. $P<0.05$ was considered to indicate statistical significance. Intraclass correlation coefficients (ICCs) were calculated to assess the interobserver variability (23). All data analyses were performed using RStudio version 1.2.1335.

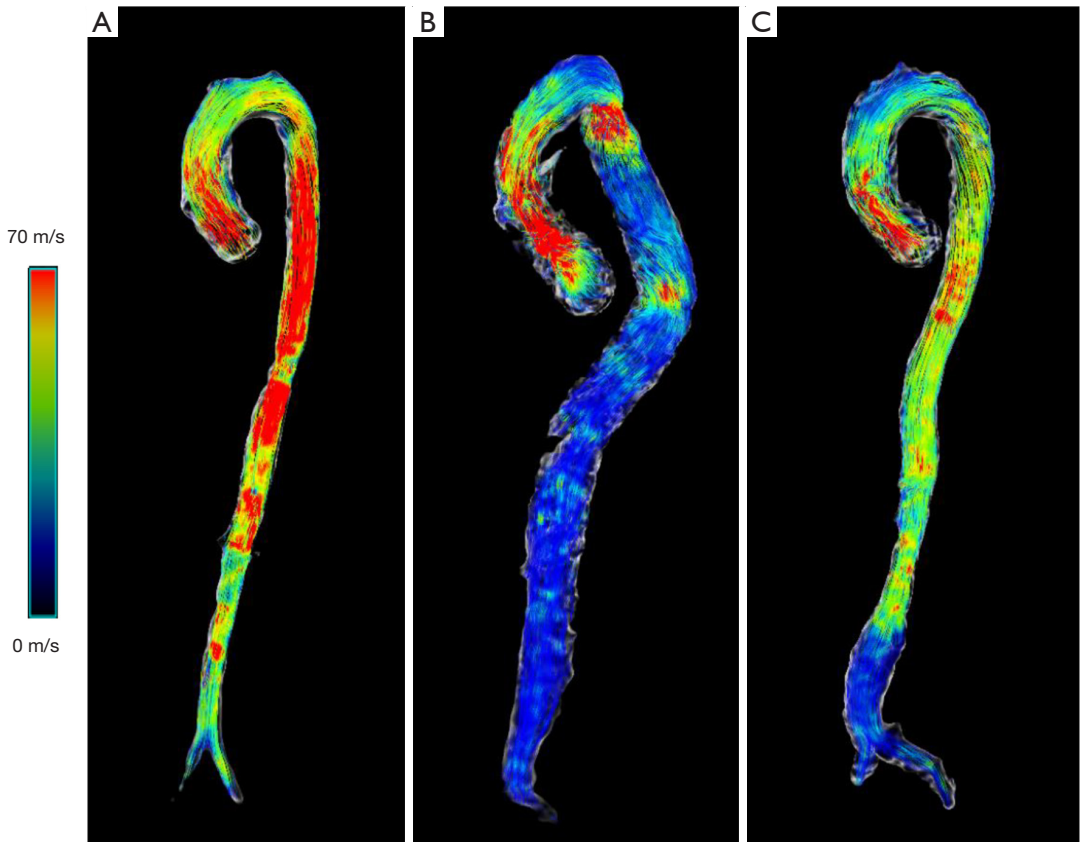

Figure 2 Streamline image of the whole aorta at systole illustrating different flow patterns among (A) age- and sex-matched controls, (B) patients with TAAA, and (C) patients with AAA. TAAA, thoracoabdominal aortic aneurysm; AAA, abdominal aortic aneurysm.

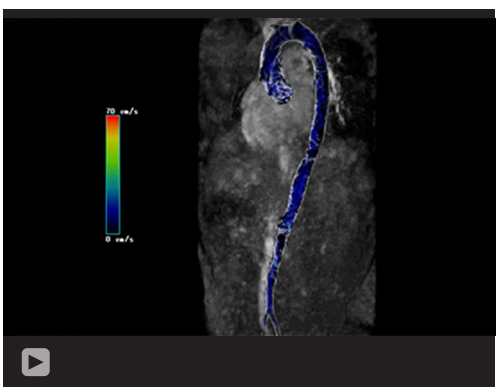

Video 1 Visualization of streamline flow in healthy volunteers.

Results

Baseline characteristics

This study included 11 patients with TAAA, 19 patients with AAA, and 21 control volunteers. The flow diagram of patient selection is shown in the Figure S2. The mean age of the included population was 55.90±12.17 years old, with the majority of participants being male (88.24%). Details of the baseline data, anatomical parameters, and scanning data are provided in Table S1. Results for the interobserver variability of the hemodynamic parameters are shown in Table S2.

4D blood flow pattern

In healthy controls without aortic dilation or tortuosity, the main blood flow pattern of the thoracic aorta was characterized by a helical or laminar flow in the ascending aorta and aortic arch and a laminar flow in the descending aorta and abdominal aorta (*Figure 2A* and *Video 1*). The RF was low in the aortic arch and descending aorta (from the origin of the BCT to the level of the celiac trunk), with the median RF ranging from 0.1% to 1.8%.

By comparison, patients with TAAA predominantly had

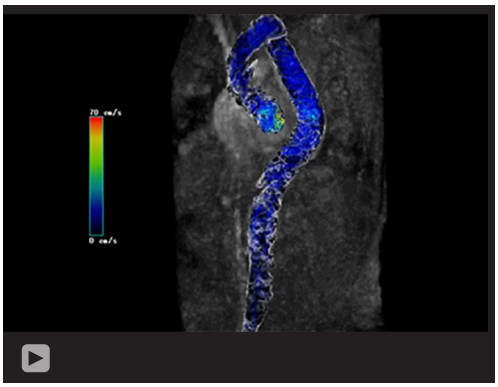

Video 2 Visualization of streamline flow in patients with TAAA. TAAA, thoracoabdominal aortic aneurysm.

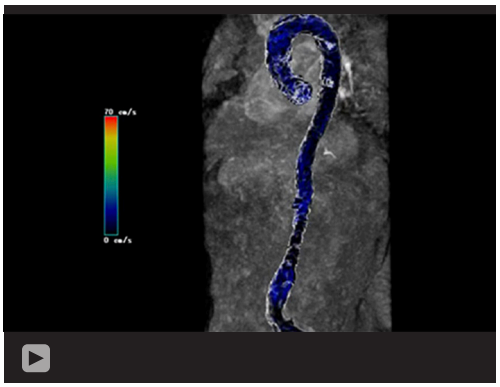

Video 3 Visualization of streamline flow in patients with AAA. AAA, abdominal aortic aneurysm.

a vortical flow or the combination of a vortical flow, helical flow, and turbulent flow in the ascending aorta and aortic arch, with part of the descending or abdominal aorta being dilated (*Figure 2B* and *Video 2*). In the thoracic segment, patients with TAAA had a significantly higher RF than did those in the control group at the planes of the BCT (TAAA: median 8.04%, IQR 3.75–15.30%; control: median 1.83%, IQR 0.39–6.75%; P=0.013), LCCA (TAAA: median 14.61%, IQR 2.98–34.58%; control: median 0.15%, IQR 0.00–1.99%; P=0.006), and LSA (median 9.64%, IQR 2.56–32.92%; control: median 1.15%, IQR 0.00–2.38%; P=0.02).

Patients with AAA also displayed vortical flow, helical flow, and turbulent flow in the ascending aorta, aortic arch, descending aorta, and dilated section of the abdominal aorta (*Figure 2C* and *Video 3*), along with a significantly higher RF at the planes of the LCCA and diaphragm (*Table 1*). A higher RF was observed in patients with AAA at the plane of aortic bifurcation compared to controls (AAA: median 19.61%, IQR 10.31–39.35%; control: median 9.97%, IQR 3.92–18.80%; P=0.046).

Table 1 Basic flow parameters of the whole aorta in the three cohorts

Aortic plane	TAAA (N=11)	AAA (N=19)	Control (N=21)	P value		
				TAAA *vs.* AAA	TAAA *vs.* control	AAA *vs.* control
Ascending aorta (root)						
TFV (mL)	51.11±15.83	57.90±20.96	55.32±16.15	0.368	0.490	0.675
V_{max} (cm/s)	131.71±23.31	123.08±23.25	140.83±34.91	0.347	0.445	0.083
RF (%)	2.55 (1.15–5.40)	3.77 (1.13–5.63)	2.30 (0.66–5.67)	0.725	0.660	0.393
Ascending aorta (middle)						
TFV (mL)	42.47±10.88	47.01±10.12	43.69±10.76	0.271	0.766	0.343
V_{max} (cm/s)	85.50±27.10	89.36±26.65	94.83±22.24	0.714	0.310	0.500
RF (%)	3.51 (2.24–15.74)	4.30 (1.99–6.89)	3.12 (0.70–5.76)	0.802	0.253	0.211
Aortic arch at the plane of the brachiocephalic trunk						
TFV (mL)	30.36±13.56	32.74±8.44	32.44±18.66	0.615	0.750	0.957
V_{max} (cm/s)	62.28±24.50	61.00±16.33	74.65±36.44	0.884	0.326	0.234
RF (%)	8.04 (3.75–15.30)	6.67 (1.65–17.27)	1.83 (0.39–6.75)	0.356	0.013	0.156

Table 1 (*continued*)

Table 1 (*continued*)

Aortic plane	TAAA (N=11)	AAA (N=19)	Control (N=21)	P value		
				TAAA *vs.* AAA	TAAA *vs.* control	AAA *vs.* control
Aortic arch at the plane of the left common carotid artery						
TFV (mL)	17.54±11.33	27.14±8.07	29.69±14.15	0.028	0.022	0.575
V_{max} (cm/s)	70.56±28.62	70.70±20.40	83.39±31.04	0.989	0.272	0.292
RF (%)	14.61 (2.98–34.58)	4.37 (2.28–9.61)	0.15 (0.00–1.99)	0.276	0.006	0.007
Aortic arch at the plane of the left subclavian artery						
TFV (mL)	17.64±9.94	29.46±11.52	28.90±10.82	0.012	0.009	0.886
V_{max} (cm/s)	62.23±23.20	66.10±20.11	74.62±16.52	0.654	0.099	0.184
RF (%)	9.64 (2.56–32.92)	1.31 (0.64–4.96)	1.15 (0.00–2.38)	0.055	0.020	0.110
Descending aorta at the plane of the pulmonary trunk bifurcation						
TFV (mL)	30.61±6.69	38.12±9.87	34.07±7.31	0.036	0.205	0.161
V_{max} (cm/s)	57.09±29.75	73.56±21.59	86.79±20.31	0.101	0.003	0.063
RF (%)	3.85 (0.03–6.91)	1.74 (0.97–3.92)	1.74 (0.08–4.05)	0.940	0.658	0.542
Descending aorta at the plane of the heart apex or diaphragm						
TFV (mL)	35.34±12.25	38.15±9.64	36.83±10.49	0.504	0.720	0.692
V_{max} (cm/s)	75.78±27.09	88.07±25.71	97.93±30.87	0.237	0.054	0.299
RF (%)	0.08 (0.00–9.98)	0.63 (0.42–3.36)	0.04 (0.00–1.51)	0.434	0.658	0.028
Abdominal aorta at the plane of the celiac trunk						
TFV (mL)	36.90±9.46	35.00±11.94	30.04±9.21	0.670	0.065	0.152
V_{max} (cm/s)	76.91±31.49	92.98±33.99	100.50±33.87	0.230	0.074	0.494
RF (%)	0.00 (0.00–0.66)	1.55 (0.13–2.86)	0.35 (0.00–2.25)	0.046	0.359	0.327
Abdominal aorta at the plane of the renal artery						
TFV (mL)	11.76±5.33	16.54±5.97	13.95±7.16	0.037	0.378	0.225
V_{max} (cm/s)	77.22±36.13	90.61±24.53	89.47±26.64	0.236	0.283	0.889
RF (%)	11.12 (8.14–26.15)	15.13 (7.49–21.07)	9.93 (3.28–15.37)	0.963	0.416	0.238
Abdominal aorta (middle of infrarenal segment)						
TFV (mL)	10.27±4.99	12.93±6.36	13.53±7.45	0.248	0.203	0.790
V_{max} (cm/s)	54.67±32.06	66.28±32.72	96.61±33.19	0.354	0.002	0.006
RF (%)	15.95 (7.27–23.40)	17.87 (6.64–25.05)	8.63 (5.17–14.26)	0.891	0.159	0.070
Abdominal aorta (aortic bifurcation)						
TFV (mL)	7.31±2.24	10.26±5.33	10.06±3.91	0.093	0.040	0.892
V_{max} (cm/s)	56.98±30.37	50.09±17.55	79.10±25.56	0.435	0.037	<0.001
RF (%)	14.65 (10.25–24.88)	19.61 (10.31–39.35)	9.97 (3.92–18.80)	0.463	0.344	0.046

TFV and V_{max} are given as the mean ± standard deviation. RF is given as the median (interquartile range). TAAA, thoracoabdominal aortic aneurysm; AAA, abdominal aortic aneurysm; TFV, total flow volume; V_{max}, maximum flow velocity; RF, regurgitation fraction.

Planar flow parameters

The V_{max} of the ascending aorta and aortic arch were similar among the patients with TAAA or AAA and controls. At the level of pulmonary trunk bifurcation, the V_{max} was significantly lower in the patients with TAAA than in the controls (57.09±29.75 *vs.* 86.79±20.31 cm/s; P=0.003). In the abdominal segment, the V_{max} was significantly lower in the patients with TAAA or AAA than it was in the controls at the planes of middle of infrarenal segment (TAAA *vs.* control: 54.67±32.06 *vs.* 96.61±33.19 cm/s, P=0.002; AAA *vs.* control: 66.28±32.72 *vs.* 96.61±33.19 cm/s, P=0.006) and aortic bifurcation (TAAA *vs.* control: 56.98±30.37 *vs.* 79.10±25.56 cm/s, P=0.037; AAA *vs.* control: 50.09±17.55 *vs.* 79.10±25.56 cm/s, P<0.001). We did not observe a significant difference in V_{max} in any plane between the patients with TAAA and AAA.

Patients with TAAA had a significantly lower TFV in the plane of the LCCA and LSA compared to patients with AAA and controls, respectively. Detailed results are summarized in *Table 1*.

Planar WSS parameters

Patients with TAAA had a significantly lower overall WSS that did the controls at all planes of aorta except for the root of the aorta (*Table 2*). In patients with TAAA, the major area of low WSS, as indicated by WSS_{max} (the maximum value of WSS in this ROI), was located around the planes of the pulmonary artery bifurcation (TAAA *vs.* control: P<0.001) and the middle infrarenal planes (TAAA *vs.* control: P<0.001). Similarly, patients with AAA also had a lower overall WSS_{max} in the ascending and descending thoracic aorta and abdominal aorta. The aortic root and aortic arch were the main segments with a similar overall WSS_{max} between patients with AAA and controls (*Table 2*). The whole-aortic mapping of WSS among the three groups is presented in *Figure 3* and *Videos 4-6*.

In addition to overall WSS, lower cir-WSS_{avg} and lower axi-WSS_{avg} were also noted in patients with TAAA compared to controls, being mainly present in the middle of the ascending aorta and whole segments of the descending and abdominal aorta. At the planes of pulmonary trunk, celiac trunk, and renal artery, patients with TAAA showed significantly lower axi-WSS_{avg} and axi-WSS_{max} compared to patients with AAA and controls. In patients with AAA, the lower axi-WSS_{avg} and cir-WSS_{avg} regions were at the planes of the aortic root, pulmonary trunk bifurcation, celiac trunk, and distal abdominal aorta. The full details of axi- and cir-WSS for each plane are shown in Table S3.

Segmental hemodynamic parameters

Both patients with TAAA and AAA had a significantly higher PWV in the thoracic aorta compared to controls. No significant difference was observed between those with TAAA or AAA and controls in terms of the PWV of the whole aorta and abdominal aorta (*Table 3*).

Pertaining to energy loss of blood flow throughout the aorta, compared to controls, patients with TAAA had a significantly higher VEL_{max} in the full-length aorta (TAAA *vs.* control: P=0.027) and abdominal aorta (TAAA *vs.* control: P=0.013). Meanwhile, in patients with AAA, a higher VEL_{max} compared to controls was only observed in the abdominal aorta (AAA *vs.* control: P=0.025). Through the geometric mapping of the VEL alongside the entire aorta (*Figure 4* and *Videos 7-9*), we found that the VEL mainly increased around the aneurysm neck or kinked aorta, which was followed by a varied nonlaminar flow in the downstream aorta.

Discussion

To the best of our knowledge, this is the first study to examine the hemodynamics of the whole aorta in patients with TAAA based on 4D flow MRI. When compared to the age- and sex-matched aortic-healthy volunteers, the hemodynamic pattern of TAAA was characterized by (I) a higher RF and lower peak velocity in the dilated plane, (II) a lower WSS almost alongside the whole range of the aorta, (III) a higher PWV in the thoracic aorta, and (IV) greater VEL in the whole aorta and abdominal aorta.

Both patients with TAAA and AAA predominantly showed vortical or turbulent flow in the dilated part of the descending or abdominal aorta, with a higher RF and a lower V_{max}. This is consistent with a previous 4D flow MRI study, which also noted flow stasis in the dilated abdominal aorta of patients with AAA, characterized by a longer volumetric residence time and lower flow velocity (24,25). However, related studies have primarily concentrated on the local hemodynamic changes of the dilated part of aorta; in contrast, our study also examined the areas upstream and downstream of the dilation in the whole aorta. Apart from the local abnormal flow pattern, we also found dominant vortical flow or turbulent flow in the ascending aorta of

Table 2 Wall shear stress of 11 regions of interest from the whole aorta in the three cohorts

Aortic plane	TAAA (N=11)	AAA (N=19)	Control (N=21)	P value		
				TAAA *vs.* AAA	TAAA *vs.* control	AAA *vs.* control
Ascending aorta (root)						
WSS_{max} (Pa)	0.15 (0.13–0.19)	0.15 (0.12–0.20)	0.17 (0.13–0.22)	0.981	0.635	0.329
WSS_{avg} (Pa)	0.06 (0.06–0.08)	0.06 (0.05–0.07)	0.07 (0.06–0.09)	0.465	0.311	0.041
Ascending aorta (middle)						
WSS_{max} (Pa)	0.13 (0.10–0.16)	0.12 (0.11–0.16)	0.17 (0.15–0.20)	0.778	0.023	0.027
WSS_{avg} (Pa)	0.06 (0.05–0.06)	0.06 (0.05–0.07)	0.07 (0.06–0.08)	0.572	0.019	0.015
Aortic arch at the plane of the brachiocephalic trunk						
WSS_{max} (Pa)	0.12 (0.10–0.13)	0.14 (0.12–0.17)	0.17 (0.14–0.20)	0.124	0.008	0.092
WSS_{avg} (Pa)	0.05 (0.03–0.06)	0.05 (0.04–0.06)	0.07 (0.05–0.08)	0.372	0.009	0.019
Aortic arch at the plane of the left common carotid artery						
WSS_{max} (Pa)	0.13 (0.10–0.16)	0.15 (0.13–0.18)	0.18 (0.17–0.22)	0.389	0.013	0.077
WSS_{avg} (Pa)	0.05 (0.04–0.06)	0.05 (0.04–0.06)	0.07 (0.06–0.09)	0.853	0.019	0.005
Aortic arch at the plane of the left subclavian artery						
WSS_{max} (Pa)	0.11 (0.09–0.17)	0.15 (0.13–0.19)	0.18 (0.15–0.24)	0.079	0.011	0.087
WSS_{avg} (Pa)	0.04 (0.03–0.06)	0.05 (0.04–0.06)	0.07 (0.05–0.09)	0.311	0.003	0.003
Descending aorta at the plane of the pulmonary trunk bifurcation						
WSS_{max} (Pa)	0.13 (0.09–0.14)	0.21 (0.19–0.24)	0.26 (0.21–0.34)	<0.001	<0.001	0.035
WSS_{avg} (Pa)	0.04 (0.03–0.05)	0.06 (0.05–0.08)	0.08 (0.06–0.11)	0.009	<0.001	0.015
Descending aorta at the plane of the heart apex or diaphragm						
WSS_{max} (Pa)	0.16 (0.10–0.24)	0.31 (0.24–0.35)	0.39 (0.34–0.48)	0.01	0.003	0.043
WSS_{avg} (Pa)	0.06 (0.05–0.08)	0.09 (0.07–0.10)	0.12 (0.10–0.14)	0.059	0.002	0.007
Abdominal aorta at the plane of the celiac trunk						
WSS_{max} (Pa)	0.12 (0.10–0.19)	0.32 (0.25–0.39)	0.44 (0.36–0.53)	<0.001	<0.001	0.006
WSS_{avg} (Pa)	0.06 (0.04–0.07)	0.10 (0.07–0.12)	0.14 (0.12–0.17)	<0.001	<0.001	0.003
Abdominal aorta at the plane of the renal artery						
WSS_{max} (Pa)	0.22 (0.13–0.27)	0.35 (0.32–0.46)	0.46 (0.37–0.62)	0.001	<0.001	0.025
WSS_{avg} (Pa)	0.07 (0.06–0.08)	0.10 (0.08–0.12)	0.13 (0.11–0.16)	0.006	<0.001	0.01
Abdominal aorta (middle of infrarenal segment)						
WSS_{max} (Pa)	0.10 (0.05–0.34)	0.12 (0.08–0.14)	0.47 (0.38–0.55)	0.914	<0.001	<0.001
WSS_{avg} (Pa)	0.04 (0.02–0.08)	0.05 (0.04–0.06)	0.14 (0.12–0.16)	0.438	<0.001	<0.001
Abdominal aorta (aortic bifurcation)						
WSS_{max} (Pa)	0.15 (0.09–0.34)	0.18 (0.11–0.26)	0.44 (0.36–0.50)	0.796	0.002	<0.001
WSS_{avg} (Pa)	0.05 (0.03–0.08)	0.05 (0.04–0.07)	0.13 (0.11–0.15)	0.590	<0.001	<0.001

All data are given as the median (interquartile range). TAAA, thoracoabdominal aortic aneurysm; AAA, abdominal aortic aneurysm; WSS_{max}, maximum overall wall shear stress; WSS_{avg}, average overall wall shear stress.

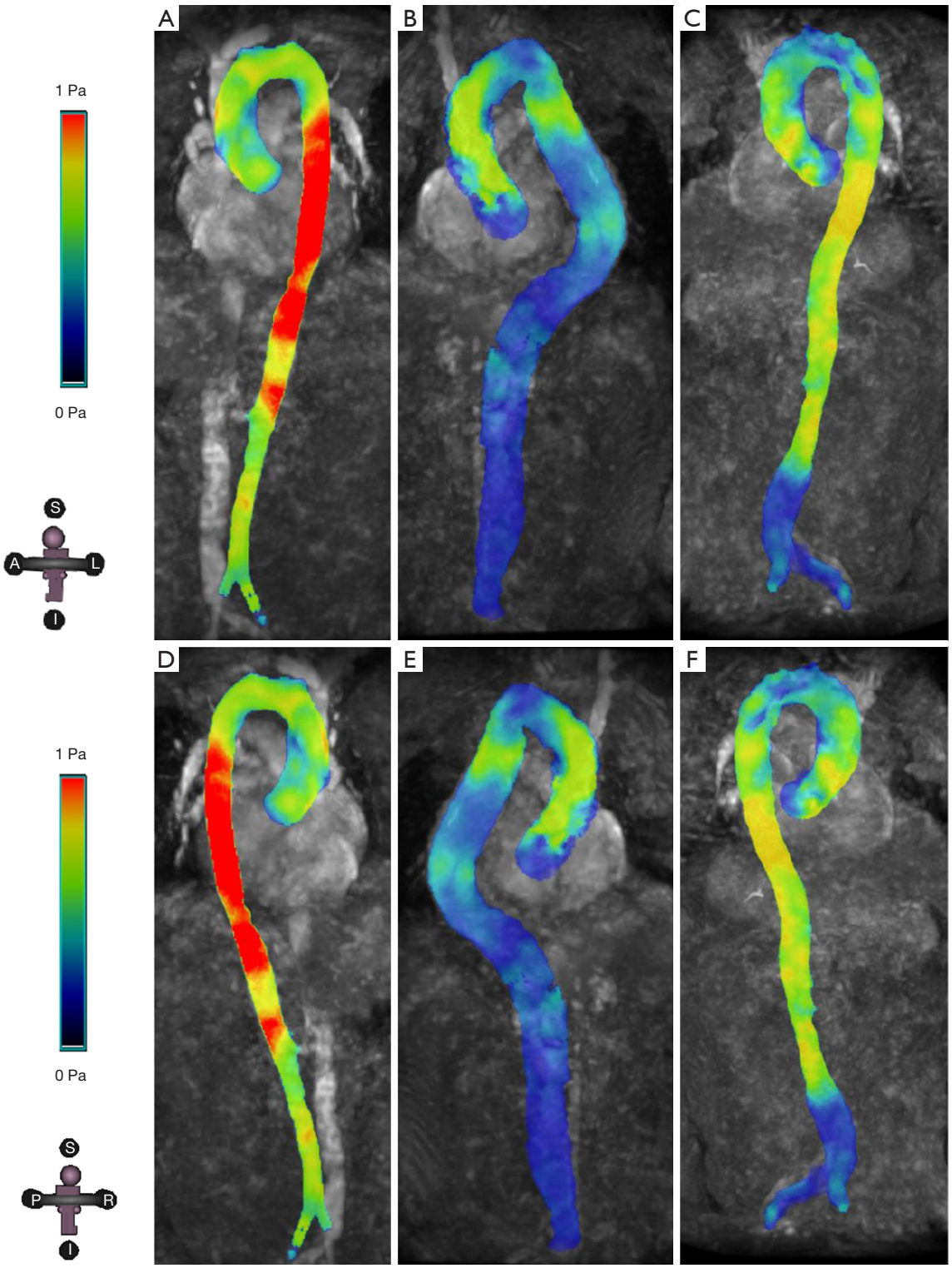

Figure 3 WSS of the whole aorta. The first row is the left-anterior oblique view (A-C), and the second row is right-anterior oblique view (D-F). (A,D) Age- and sex-matched controls, (B,E) patients with TAAA, and (C,F) patients with AAA. A, P, L, R, S and I indicate the position of the human body. S, superior; I, inferior; A, anterior; P, posterior; L, left; R, right; WSS, wall shear stress; TAAA, thoracoabdominal aortic aneurysm; AAA, abdominal aortic aneurysm.

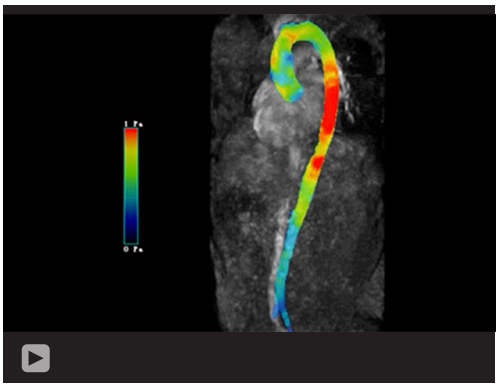

Video 4 Visualization of WSS in healthy volunteers. WSS, wall shear stress.

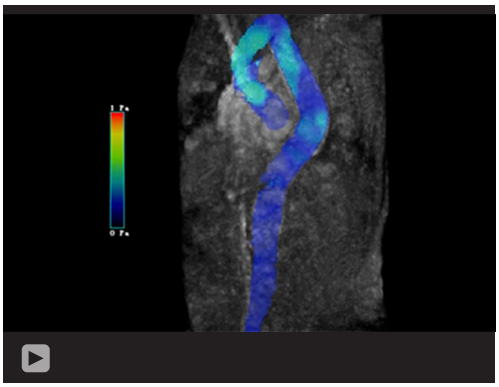

Video 5 Visualization of WSS in patients with TAAA. WSS, wall shear stress; TAAA, thoracoabdominal aortic aneurysm.

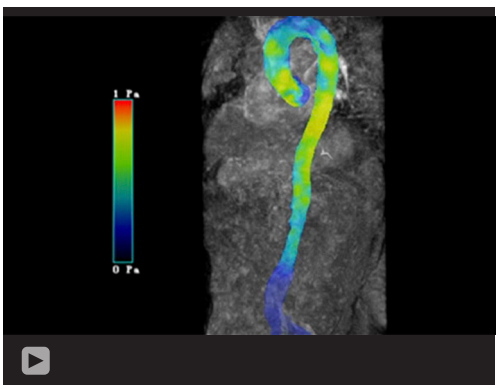

Video 6 Visualization of WSS in patients with AAA. WSS, wall shear stress; AAA, abdominal aortic aneurysm.

patients with TAAA or AAA, which can likely be attributed the larger diameter of the ascending aorta in these two groups. Thus, downstream aortic dilation pathologies can alter the upstream blood flow pattern and dynamics to some degree.

In addition to regurgitation, VEL, a more comprehensive and advanced parameter, was evaluated to reflect the irreversible loss of mechanical kinetic energy caused by friction due to fluid viscosity and the no-slip condition (20). In examining the VEL distribution among the three groups, we found that regions with high VEL usually had an origin of nonlaminar flow, including vortical, turbulent, and helical flows, which may indicate that VEL can act as a good hemodynamic marker to quantify the degree of nonlaminar flow via the dimension of transition from kinetic energy to thermal energy. Moreover, a similar energy parameter, turbulent kinetic energy, has also been used to describe the fluctuation in kinetic energy during turbulence, but it has more often been used in high Reynolds numbers for poststenotic flow (26,27). VEL has also been reported to be a good marker for assessing the increased cardiac afterload induced by an abnormal downstream nonlaminar blood flow (20,28,29). In a previous pilot study, VEL was shown to be elevated in patients with aortic dilation compared to controls, which was associated with the increased cardiac afterload (21). Similar findings were also noted in the study by Han and colleagues, in which VEL was found to be an indicator for pulmonary hypertension (30). In our study, significantly elevated VEL was observed in the entire aorta of patients with TAAA, which suggested the abnormal increased workload of every heartbeat. This suggests a need to pay attention to the potential long-term major adverse cardiac events of patients with TAAA, especially adverse ventricle remodeling resulting from a heavier afterload.

The biomechanical nature of the aortic wall was also evaluated in our study through two aspects: (I) the aortic stiffness assessed via PWV and (II) the dilation tendency of the aorta assessed via WSS. It has been acknowledged that the PWV generated by 4D flow MRI can accurately reflect the stiffness of the aorta with full 3D aortic coverage (31). Jarvis *et al.* reported that the aortic PWV increases with age by approximately 1 m/s per decade and that a high PWV can result in a decline in cardiac function and reduced downstream flow velocity (18). The results of our study revealed that both patients with TAAA and AAA

Table 3 Advanced segmental hemodynamic parameters from the three cohorts

Aortic segment	TAAA (N=11)	AAA (N=19)	Control (N=21)	P value		
				TAAA *vs.* AAA	TAAA *vs.* control	AAA *vs.* control
Whole aorta						
PWV (m/s)	8.05 (5.07–10.64)	7.29 (6.22–9.46)	6.78 (5.33–8.64)	0.847	0.821	0.531
VEL_{max} (μW/mm^2)	22.95 (10.06–29.39)	15.68 (9.84–21.01)	12.29 (8.71–13.80)	0.175	0.027	0.101
VEL_{avg} (μW/mm^2)	5.57 (4.16–9.21)	4.94 (3.13–6.03)	5.33 (3.81–7.03)	0.139	0.505	0.32
Thoracic aorta						
PWV (m/s)	11.41 (9.56–14.32)	8.75 (7.35–10.75)	7.21 (5.57–7.79)	0.069	<0.001	0.024
VEL_{max} (μW/mm^2)	9.30 (4.13–18.61)	8.25 (5.32–10.91)	5.60 (5.05–9.25)	0.557	0.353	0.428
VEL_{avg} (μW/mm^2)	2.34 (1.82–4.96)	2.13 (1.57–2.44)	2.35 (1.70–3.18)	0.301	0.353	0.465
Abdominal aorta						
PWV (m/s)	5.39 (3.50–7.06)	5.97 (2.22–9.71)	6.40 (3.18–8.91)	0.717	0.539	0.771
VEL_{max} (μW/mm^2)	2.99 (2.14–5.75)	2.74 (1.88–3.97)	1.66 (1.09–2.44)	0.715	0.013	0.025
VEL_{avg} (μW/mm^2)	0.54 (0.36–0.93)	0.71 (0.50–1.28)	0.64 (0.41–0.80)	0.393	0.858	0.331

All data are given as the median (interquartile range). TAAA, thoracoabdominal aortic aneurysm; AAA, abdominal aortic aneurysm; PWV, pulse wave velocity; VEL_{max}, maximum viscous energy loss; VEL_{avg}, average viscous energy loss.

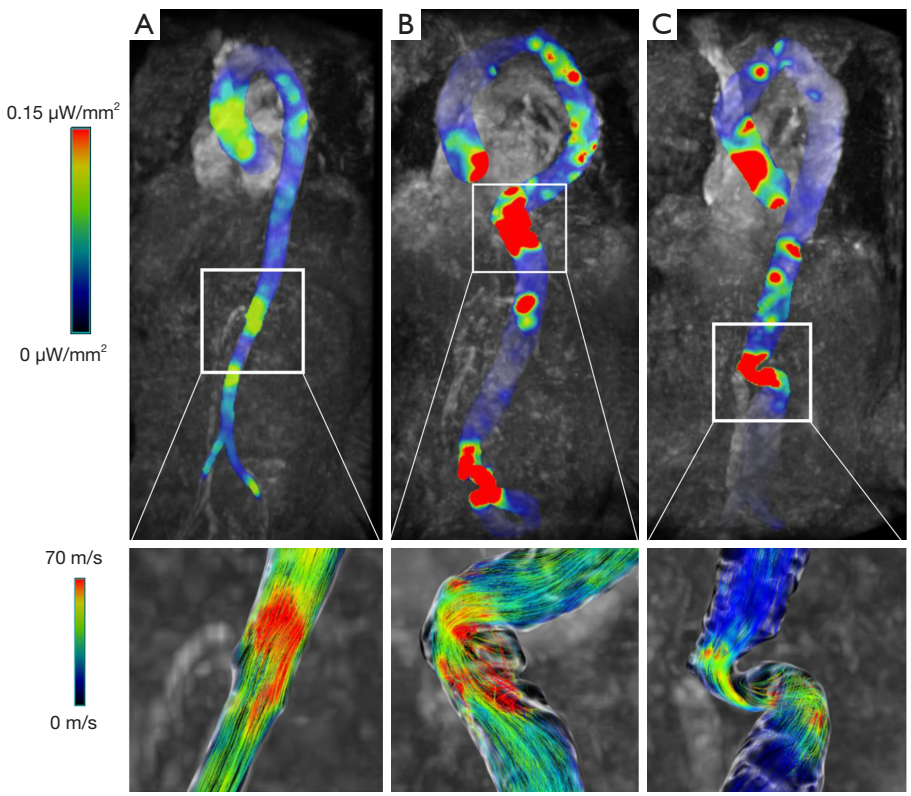

Figure 4 Mapping of VEL among (A) age- and sex-matched controls, (B) patients with TAAA, and (C) patients with AAA. The first row shows the whole aorta. The second row shows the locally enlarged streamline diagrams of the areas with increased VEL. VEL, viscous energy loss; TAAA, thoracoabdominal aortic aneurysm; AAA, abdominal aortic aneurysm.

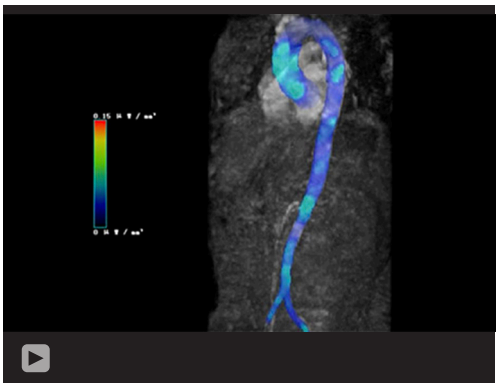

Video 7 Visualization of VEL in healthy volunteers. VEL, viscous energy loss.

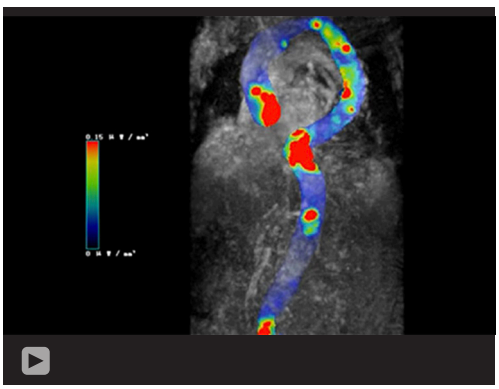

Video 8 Visualization of VEL in patients with TAAA. VEL, viscous; energy loss; TAAA, thoracoabdominal aortic aneurysm.

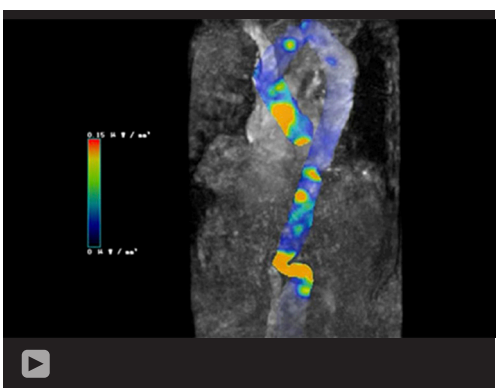

Video 9 Visualization of VEL in patients with AAA. VEL, viscous energy loss; AAA, abdominal aortic aneurysm.

had a significantly higher PWV than did the age- and sex-matched healthy volunteers, which suggests these patients had stiffer aortas, probably due to the dilated aortic wall and intramural thrombus. The higher PWV in the patients with TAAA and AAA was accompanied by a lower peak velocity in the downstream abdominal aorta. Moreover, both higher PWV and higher VEL suggested an increased risk of cardiac function insufficiency in patients with TAAA and AAA. Regarding the tendency of aortic dilation, WSS is considered to be a classic hemodynamic marker and has been verified in multiple studies (32,33). Evidence suggests that after decomposition into two directions, both axial and circumferential WSS can independently predict proximal descending aorta dilation beyond clinical factors (34). In the present study, the WSS was lower in patients with TAAA than in controls in nearly each plane of the whole aorta, even at areas without obvious dilation. Similar findings were observed in patients with AAA, with WSS being lower both in the abdominal aorta and in the ascending and descending aorta. Our results suggest that the whole aortic wall of the patients with TAAA or AAA was at the risk of dilation, regardless of the diameter.

Despite the superiority and novelty of the whole-aorta 4D flow technique, our study nonetheless involved several limitations that should be addressed. First, the sample size of our study was relatively small, but this was a cross-sectional population of selected participants from a prospective, nested, case-control study (trial registration number: ChiCTR2100054252). Our results need to be further validated by further research. Second, the selection of the VENC value in our study was based on the 2D PC velocity of the descending aorta at the level of the diaphragm, which was different from other studies. However, our results indicated that the velocity at this level almost represented the highest flow rate in the scanning view. Moreover, the good image quality further justified our method. Third, there was innate clinical heterogeneity across the three groups in terms of age, gender, BMI, comorbidities, etc., but age and sex matching was completed among the TAAA, AAA, and control groups to minimize the influence of confounders.

Conclusions

Compared to age- and sex-matched healthy volunteers,

patients with TAAA had a stiffer aortic wall and tended to have dilation alongside the whole aorta, which was accompanied by an abnormal flow pattern, with a higher RF and a lower peak velocity in the dilated part. High WEL in the entire aorta stood out as a prominent and unique marker of abnormal hemodynamics in patients with TAAA. Future research is required to determine whether the above parameters can help to predict TAAA growth and rupture.

Acknowledgments

Funding: This work was funded by grants from the National Natural Science Foundation of China (grant Nos. 82371927, 82302152, and 82300542), the Sichuan Province Science and Technology Support Program (grant Nos. 2022YFS0366, 2022YFS0187, and 2022YFS0359), and the National Key R&D Program of China (grant No. 2022YFC2009905).

Footnote

Reporting Checklist: The authors have completed the STROBE reporting checklist. Available at https://qims.amegroups.com/article/view/10.21037/qims-23-1321/rc

Conflicts of Interest: All authors have completed the ICMJE uniform disclosure form (available at https://qims.amegroups.com/article/view/10.21037/qims-23-1321/coif). J.W. received funding from the National Natural Science Foundation of China (grant Nos. 82371927, 82302152, and 82300542), the Sichuan Province Science and Technology Support Program (grant Nos. 2022YFS0366, 2022YFS0187, and 2022YFS0359). Z.L. received funding from the National Natural Science Foundation of China (grant Nos. 82371927, 82302152, and 82300542), and the National Key R&D Program of China (grant No. 2022YFC2009905). The other authors have no conflicts of interest to declare.

Ethical Statement: The authors are accountable for all aspects of the work in ensuring that questions related to the accuracy or integrity of any part of the work are appropriately investigated and resolved. This study was conducted in accordance with the Declaration of Helsinki (as revised in 2013) and was approved by ethics committee of West China Hospital, Sichuan University (reference number 2021-1171). Informed consent was obtained from all individual participants.

References

1. Frederick JR, Woo YJ. Thoracoabdominal aortic aneurysm. Ann Cardiothorac Surg 2012;1:277-85.
2. Hiratzka LF, Bakris GL, Beckman JA, Bersin RM, Carr VF, Casey DE Jr, et al. 2010 ACCF/AHA/AATS/ACR/ASA/SCA/SCAI/SIR/STS/SVM guidelines for the diagnosis and management of patients with Thoracic Aortic Disease: a report of the American College of Cardiology Foundation/American Heart Association Task Force on Practice Guidelines, American Association for Thoracic Surgery, American College of Radiology, American Stroke Association, Society of Cardiovascular Anesthesiologists, Society for Cardiovascular Angiography and Interventions, Society of Interventional Radiology, Society of Thoracic Surgeons, and Society for Vascular Medicine. Circulation 2010;121:e266-369.
3. Kim JB, Kim K, Lindsay ME, MacGillivray T, Isselbacher EM, Cambria RP, Sundt TM 3rd. Risk of rupture or dissection in descending thoracic aortic aneurysm. Circulation 2015;132:1620-9.
4. Oda T, Minatoya K, Sasaki H, Tanaka H, Seike Y, Itonaga T, Inoue Y, Higashi M, Nishimura K, Kobayashi J. Surgical Indication for Chronic Aortic Dissection in Descending Thoracic and Thoracoabdominal Aorta. Circ Cardiovasc Interv 2017;10:e004292.
5. Zafar MA, Chen JF, Wu J, Li Y, Papanikolaou D, Abdelbaky M, Faggion Vinholo T, Rizzo JA, Ziganshin BA, Mukherjee SK, Elefteriades JA; Yale Aortic Institute Natural History Investigators. Natural history of descending thoracic and thoracoabdominal aortic aneurysms. J Thorac Cardiovasc Surg 2021;161:498-511.e1.
6. Zhang M, Peng F, Tong X, Feng X, Li Y, Chen H, Niu H, Zhang B, Song G, Li Y, Liu P, Liu A, Li R. Associations between haemodynamics and wall enhancement of intracranial aneurysm. Stroke Vasc Neurol 2021;6:467-75.
7. Kojima K, Hiro T, Koyama Y, Ohgaku A, Fujito H,

Ebuchi Y, et al. High Wall Shear Stress Is Related to Atherosclerotic Plaque Rupture in the Aortic Arch of Patients with Cardiovascular Disease: A Study with Computational Fluid Dynamics Model and Non-Obstructive General Angioscopy. J Atheroscler Thromb 2021;28:742-53.
8. Boyd AJ, Kuhn DC, Lozowy RJ, Kulbisky GP. Low wall shear stress predominates at sites of abdominal aortic aneurysm rupture. J Vasc Surg 2016;63:1613-9.
9. Pereira VM, Brina O, Bijlenga P, Bouillot P, Narata AP, Schaller K, Lovblad KO, Ouared R. Wall shear stress distribution of small aneurysms prone to rupture: a case-control study. Stroke 2014;45:261-4.
10. Morris PD, Narracott A, von Tengg-Kobligk H, Silva Soto DA, Hsiao S, Lungu A, Evans P, Bressloff NW, Lawford PV, Hose DR, Gunn JP. Computational fluid dynamics modelling in cardiovascular medicine. Heart 2016;102:18-28.
11. Schwarz EL, Pegolotti L, Pfaller MR, Marsden AL. Beyond CFD: Emerging methodologies for predictive simulation in cardiovascular health and disease. Biophys Rev (Melville) 2023;4:011301.
12. Shah DJ. 4D Flow CMR: The Final Frontier in Valvular Heart Disease? JACC Cardiovasc Imaging 2021;14:1367-8.
13. Secinaro A, Milano EG, Ciancarella P, Trezzi M, Capelli C, Ciliberti P, Cetrano E, Curione D, Santangelo TP, Napolitano C, Albanese SB, Carotti A. Blood flow characteristics after aortic valve neocuspidization in paediatric patients: a comparison with the Ross procedure. Eur Heart J Cardiovasc Imaging 2022;23:275-82.
14. Spampinato RA, Jahnke C, Crelier G, Lindemann F, Fahr F, Czaja-Ziolkowska M, Sieg F, Strotdrees E, Hindricks G, Borger MA, Paetsch I. Quantification of regurgitation in mitral valve prolapse with four-dimensional flow cardiovascular magnetic resonance. J Cardiovasc Magn Reson 2021;23:87.
15. Spartera M, Pessoa-Amorim G, Stracquadanio A, Von Ende A, Fletcher A, Manley P, Neubauer S, Ferreira VM, Casadei B, Hess AT, Wijesurendra RS. Left atrial 4D flow cardiovascular magnetic resonance: a reproducibility study in sinus rhythm and atrial fibrillation. J Cardiovasc Magn Reson 2021;23:29.
16. Ebel S, Köhler B, Aggarwal A, Preim B, Behrendt B, Jung B, Gohmann RF, Riekena B, Borger M, Lurz P, Denecke T, Grothoff M, Gutberlet M. Comparison of aortic blood flow rotational direction in healthy volunteers and patients with bicuspid aortic valves using volumetric velocity-sensitive cardiovascular magnetic resonance imaging. Quant Imaging Med Surg 2023;13:7973-86.
17. Sotelo J, Dux-Santoy L, Guala A, Rodríguez-Palomares J, Evangelista A, Sing-Long C, Urbina J, Mura J, Hurtado DE, Uribe S. 3D axial and circumferential wall shear stress from 4D flow MRI data using a finite element method and a laplacian approach. Magn Reson Med 2018;79:2816-23.
18. Jarvis K, Scott MB, Soulat G, Elbaz MSM, Barker AJ, Carr JC, Markl M, Ragin A. Aortic Pulse Wave Velocity Evaluated by 4D Flow MRI Across the Adult Lifespan. J Magn Reson Imaging 2022;56:464-73.
19. Laffon E, Marthan R, Montaudon M, Latrabe V, Laurent F, Ducassou D. Feasibility of aortic pulse pressure and pressure wave velocity MRI measurement in young adults. J Magn Reson Imaging 2005;21:53-8.
20. Elbaz MS, van der Geest RJ, Calkoen EE, de Roos A, Lelieveldt BP, Roest AA, Westenberg JJ. Assessment of viscous energy loss and the association with three-dimensional vortex ring formation in left ventricular inflow: In vivo evaluation using four-dimensional flow MRI. Magn Reson Med 2017;77:794-805.
21. Barker AJ, van Ooij P, Bandi K, Garcia J, Albaghdadi M, McCarthy P, Bonow RO, Carr J, Collins J, Malaisrie SC, Markl M. Viscous energy loss in the presence of abnormal aortic flow. Magn Reson Med 2014;72:620-8.
22. Shan Y, Li J, Wu B, Barker AJ, Markl M, Lin J, Shu X, Wang Y. Aortic Viscous Energy Loss for Assessment of Valve-related Hemodynamics in Asymptomatic Severe Aortic Stenosis. Radiol Cardiothorac Imaging 2022;4:e220010.
23. Koo TK, Li MY. A Guideline of Selecting and Reporting Intraclass Correlation Coefficients for Reliability Research. J Chiropr Med 2016;15:155-63.
24. Takehara Y. Clinical Application of 4D Flow MR Imaging for the Abdominal Aorta. Magn Reson Med Sci 2022;21:354-64.
25. Ziegler M, Welander M, Lantz J, Lindenberger M, Bjarnegård N, Karlsson M, Ebbers T, Länne T, Dyverfeldt P. Visualizing and quantifying flow stasis in abdominal aortic aneurysms in men using 4D flow MRI. Magn Reson Imaging 2019;57:103-10.
26. Garcia J, Barker AJ, Markl M. The Role of Imaging of Flow Patterns by 4D Flow MRI in Aortic Stenosis. JACC Cardiovasc Imaging 2019;12:252-66.
27. Binter C, Gotschy A, Sündermann SH, Frank M, Tanner FC, Lüscher TF, Manka R, Kozerke S. Turbulent Kinetic Energy Assessed by Multipoint 4-Dimensional Flow Magnetic Resonance Imaging Provides Additional

Information Relative to Echocardiography for the Determination of Aortic Stenosis Severity. Circ Cardiovasc Imaging 2017;10:e005486.
28. Kamphuis VP, Roest AAW, van den Boogaard PJ, Kroft LJM, Lamb HJ, Helbing WA, Blom NA, Westenberg JJM, Elbaz MSM. Hemodynamic interplay of vorticity, viscous energy loss, and kinetic energy from 4D Flow MRI and link to cardiac function in healthy subjects and Fontan patients. Am J Physiol Heart Circ Physiol 2021;320:H1687-98.
29. Kamphuis VP, Elbaz MSM, van den Boogaard PJ, Kroft LJM, van der Geest RJ, de Roos A, Helbing WA, Blom NA, Westenberg JJM, Roest AAW. Disproportionate intraventricular viscous energy loss in Fontan patients: analysis by 4D flow MRI. Eur Heart J Cardiovasc Imaging 2019;20:323-33.
30. Han QJ, Witschey WR, Fang-Yen CM, Arkles JS, Barker AJ, Forfia PR, Han Y. Altered Right Ventricular Kinetic Energy Work Density and Viscous Energy Dissipation in Patients with Pulmonary Arterial Hypertension: A Pilot Study Using 4D Flow MRI. PLoS One 2015;10:e0138365.
31. Houriez-Gombaud-Saintonge S, Mousseaux E, Bargiotas I, De Cesare A, Dietenbeck T, Bouaou K, Redheuil A, Soulat G, Giron A, Gencer U, Craiem D, Messas E, Bollache E, Chenoune Y, Kachenoura N. Comparison of different methods for the estimation of aortic pulse wave velocity from 4D flow cardiovascular magnetic resonance. J Cardiovasc Magn Reson 2019;21:75.
32. Kiema M, Sarin JK, Kauhanen SP, Torniainen J, Matikka H, Luoto ES, Jaakkola P, Saari P, Liimatainen T, Vanninen R, Ylä-Herttuala S, Hedman M, Laakkonen JP. Wall Shear Stress Predicts Media Degeneration and Biomechanical Changes in Thoracic Aorta. Front Physiol 2022;13:934941.
33. Guala A, Dux-Santoy L, Teixido-Tura G, Ruiz-Muñoz A, Galian-Gay L, Servato ML, Valente F, Gutiérrez L, González-Alujas T, Johnson KM, Wieben O, Casas-Masnou G, Sao Avilés A, Fernandez-Galera R, Ferreira-Gonzalez I, Evangelista A, Rodríguez-Palomares JF. Wall Shear Stress Predicts Aortic Dilation in Patients With Bicuspid Aortic Valve. JACC Cardiovasc Imaging 2022;15:46-56.
34. Guala A, Teixido-Tura G, Dux-Santoy L, Granato C, Ruiz-Muñoz A, Valente F, Galian-Gay L, Gutiérrez L, González-Alujas T, Johnson KM, Wieben O, Sao Avilés A, Evangelista A, Rodriguez-Palomares J. Decreased rotational flow and circumferential wall shear stress as early markers of descending aorta dilation in Marfan syndrome: a 4D flow CMR study. J Cardiovasc Magn Reson 2019;21:63.

Cite this article as: Zeng W, Wang J, Weng C, Peng W, Wang T, Yuan D, Huang B, Zhao J, Xia C, Li Z, Guo Y. Assessment of aortic hemodynamics in patients with thoracoabdominal aortic aneurysm using four-dimensional magnetic resonance imaging: a cross-sectional study. Quant Imaging Med Surg 2024;14(4):2800-2815. doi: 10.21037/qims-23-1321

Supplementary

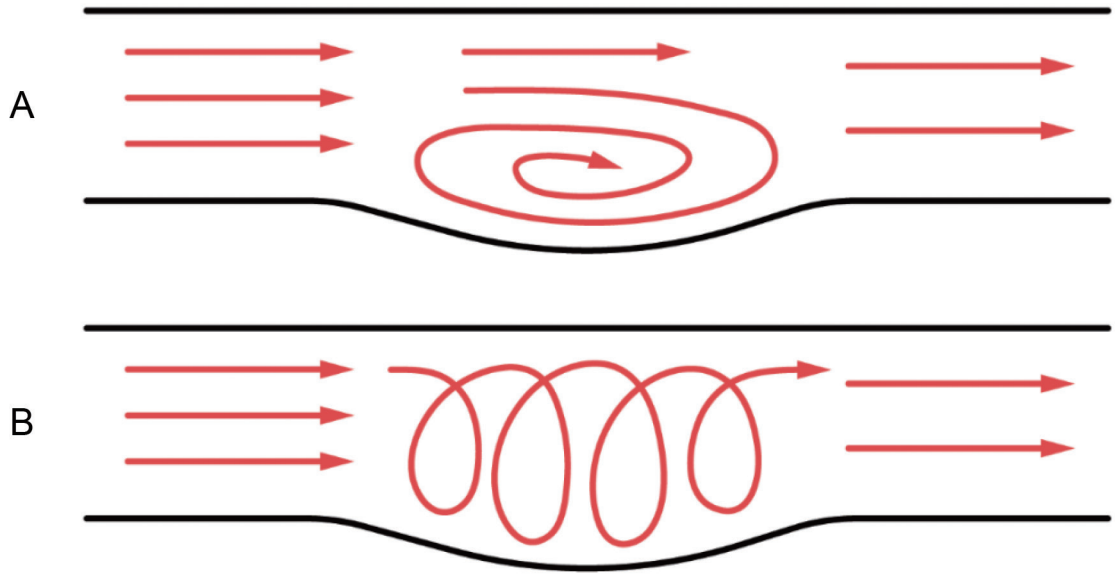

Figure S1 A sketch of vortical flow (A) and helical flow (B).

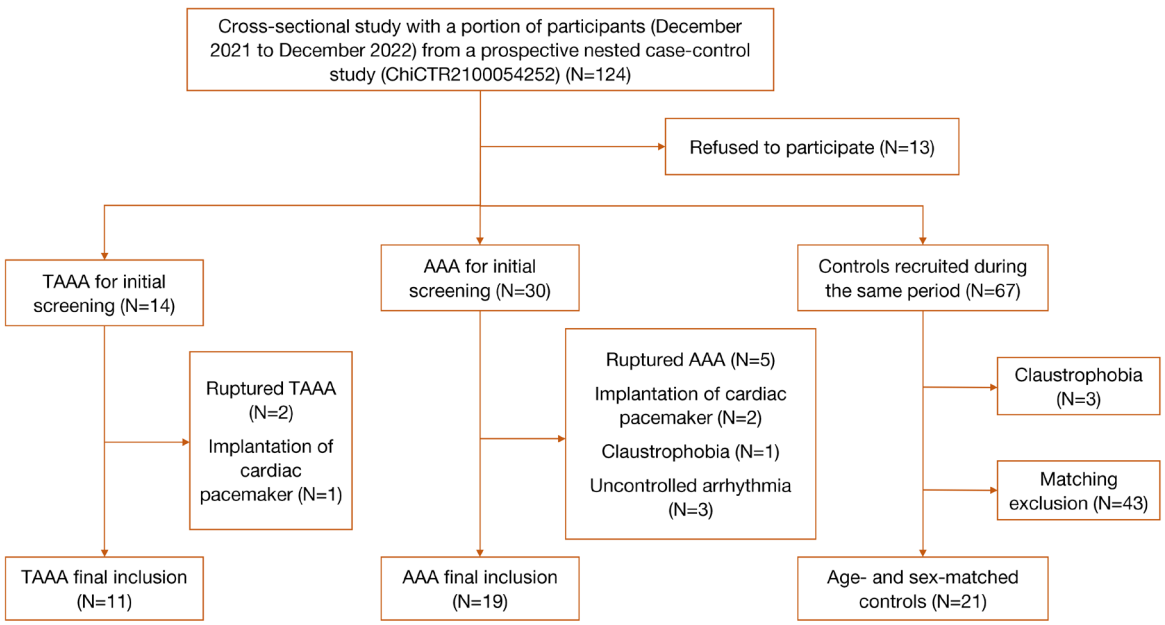

Figure S2 Flow diagram of participant selection in the study. TAAA, thoracoabdominal aortic aneurysm; AAA, abdominal aortic aneurysm.

https://dx.doi.org/10.21037/qims-23-1321

Table S1 Overview of clinical characteristics of the three cohorts

Basic information	TAAA (N=11)	AAA (N=19)	Control (N=21)	P value		
				TAAA *vs.* AAA	TAAA *vs.* control	AAA *vs.* control
Age (years)	53.18±11.90	58.00±11. 73	55.43±14.96	0.29	0.67	0.552
BMI (kg/m^2)	24.67±4.08	24.55±3.27	23.48±3.53	0.926	0.396	0.329
HR	72.64±12.59	70.32±8.25	75.84±10.26	0.546	0.454	0.076
Sex				0.603	0.998	0.654
Male	10 (90.91%)	16 (84.21%)	19 (90.48%)			
Female	1 (9.09%)	3 (15.79%)	2 (9.52%)			
HTN	4 (36.36%)	5 (26.32%)	3 (14.29%)	0.84	0.968	0.911
DM	1 (9.09%)	1 (5.26%)	3 (14.29%)	0.685	0.673	0.607
CAD	4 (36.36%)	7 (36.84%)	3 (14.29%)	0.979	0.151	0.1
Cerebrovascular	2 (18.18%)	1 (5.26%)	2 (9.52%)	0.256	0.482	0.609
COPD	1 (9.09%)	0 (0.00%)	0 (0.00%)	0.367	0.344	–
CKD	1 (9.09%)	0 (0.00%)	0 (0.00%)	0.367	–	–
CTD	3 (27.27%)	3 (15.79%)	0 (0.00%)	0.641	–	0.098
AA diameter (mm)	47.00 (44.45–58.35)	45.00 (33.15–50.00)	14.90 (13.95–17.12)	0.182	<0.001	<0.001
ASC diameter (mm)	35.00 (32.50–40.00)	36.50 (31.10–39.85)	31.20 (26.23–34.55)	0.796	0.043	0.04
LCIA diameter (mm)	12.40 (10.00–16.00)	16.10 (12.75–20.55)	9.85 (8.55–11.00)	0.048	0.022	<0.001
RCIA diameter (mm)	15.00 (10.50–18.50)	18.20 (13.65–23.95)	9.90 (8.50–11.00)	0.097	0.007	<0.001
Scan time (minutes)	7.49±1.26	7.16±1.76	6.00±1.13	0.413	0.005	0.024

Data are presented as the n (%) or mean standard deviation. Diameters are presented as the median (interquartile range). TAAA, thoracoabdominal aortic aneurysm; AAA, abdominal aortic aneurysm; BMI, body mass index; HR, heart rate; HTN, hypertension; DM, diabetes mellitus; CAD, coronary artery disease; COPD, chronic obstructive pulmonary disease; CKD, chronic kidney disease; CTD, connective tissue disease; AA, arterial aneurysm; ASC, ascending aorta; LCIA, left iliac artery; RCIA, right iliac artery.

https://dx.doi.org/10.21037/qims-23-1321

Table S2 Interobserver variability in hemodynamic parameters assessed by intraclass correlation coefficient in 10 healthy volunteers

Hemodynamic parameters of 11 ROIs	ICC	P value
Ascending aorta: root		
TFV	0.868	0.003
V_{max}	0.979	<0.001
RF	0.941	<0.001
axi-WSS_{max}	0.792	0.014
axi-WSS_{avg}	0.802	0.012
cir-WSS_{max}	0.927	<0.001
cir-WSS_{avg}	0.783	0.016
WSS_{max}	0.88	0.002
WSS_{avg}	0.997	<0.001
Ascending aorta: middle		
TFV	0.952	<0.001
V_{max}	0.582	0.105
RF	0.826	0.888
axi-WSS_{max}	0.698	0.044
axi-WSS_{avg}	0.494	0.162
cir-WSS_{max}	0.533	0.136
cir-WSS_{avg}	0.871	0.003
WSS_{max}	0.782	0.017
WSS_{avg}	0.877	0.002
Aortic arch at the plane of the brachiocephalic trunk		
TFV	0.962	<0.001
V_{max}	0.688	0.049
RF	0.768	0.02
axi-WSS_{max}	0.875	0.002
axi-WSS_{avg}	0.681	0.052
cir-WSS_{max}	0.84	0.006
cir-WSS_{avg}	0.846	0.005
WSS_{max}	0.96	<0.001
WSS_{avg}	0.937	<0.001
Aortic arch at the plane of the left common carotid artery		
TFV	0.963	<0.001
V_{max}	0.63	0.077
RF	0.777	0.018
axi-WSS_{max}	0.793	0.014
axi-WSS_{avg}	0.737	0.03
cir-WSS_{max}	0.763	0.022
cir-WSS_{avg}	0.632	0.076
WSS_{max}	0.968	<0.001
WSS_{avg}	0.955	<0.001
Aortic arch at the plane of the left subclavian artery		
TFV	0.955	<0.001
V_{max}	0.689	0.048
RF	0.974	<0.001
axi-WSS_{max}	0.735	0.031
axi-WSS_{avg}	0.841	0.006
cir-WSS_{max}	0.566	0.115
cir-WSS_{avg}	0.785	0.016
WSS_{max}	0.971	<0.001
WSS_{avg}	0.98	<0.001
Descending aorta at the plane of the pulmonary trunk bifurcation		
TFV	0.915	0.001
V_{max}	0.964	<0.001
RF	0.878	0.002
axi-WSS_{max}	0.716	0.037
axi-WSS_{avg}	0.835	0.007
cir-WSS_{max}	0.604	0.092
cir-WSS_{avg}	0.878	0.002
WSS_{max}	0.725	0.034
WSS_{avg}	0.855	0.004

https://dx.doi.org/10.21037/qims-23-1321

Table S2 (*continued*)

Hemodynamic parameters of 11 ROIs	ICC	P value
Descending aorta at the plane of the heart apex or diaphragm		
TFV	0.939	<0.001
V_{max}	0.935	<0.001
RF	0.852	0.004
axi-WSS_{max}	0.89	0.001
axi-WSS_{avg}	0.884	0.002
cir-WSS_{max}	0.679	0.053
cir-WSS_{avg}	0.842	0.006
WSS_{max}	0.975	<0.001
WSS_{avg}	0.928	<0.001
Abdominal aorta at the plane of the celiac trunk		
TFV	0.7	0.004
V_{max}	0.978	<0.001
RF	0.905	0.001
axi-WSS_{max}	0.949	<0.001
axi-WSS_{avg}	0.971	<0.001
cir-WSS_{max}	0.511	0.15
cir-WSS_{avg}	0.937	<0.001
WSS_{max}	0.959	<0.001
WSS_{avg}	0.985	<0.001
Abdominal aorta at the plane of the renal artery		
TFV	0.666	0.059
V_{max}	0.799	0.013
RF	0.615	0.086
axi-WSS_{max}	0.797	0.013
axi-WSS_{avg}	0.919	<0.001
cir-WSS_{max}	0.649	0.068
cir-WSS_{avg}	0.875	0.002
WSS_{max}	0.989	<0.001
WSS_{avg}	0.995	<0.001
Abdominal aorta: middle		
TFV	0.929	<0.001
V_{max}	0.791	0.015
RF	0.972	<0.001
axi-WSS_{max}	0.54	0.131
axi-WSS_{avg}	0.835	0.007
cir-WSS_{max}	0.521	0.144
cir-WSS_{avg}	0.752	0.025
WSS_{max}	0.891	0.001
WSS_{avg}	0.968	<0.001
Abdominal aorta: aortic bifurcation		
TFV	0.968	<0.001
V_{max}	0.791	0.014
RF	0.972	<0.001
axi-WSS_{max}	0.881	0.002
axi-WSS_{avg}	0.919	<0.001
cir-WSS_{max}	0.744	0.028
cir-WSS_{avg}	0.969	<0.001
WSS_{max}	0.955	<0.001
WSS_{avg}	0.947	<0.001
Segmental hemodynamic parameters		
Whole aorta		
PWV	0.75	0.025
VEL_{max}	0.977	<0.001
VEL_{avg}	0.976	<0.001
Thoracic aorta		
PWV	0.6	0.094
VEL_{max}	0.84	0.006
VEL_{avg}	0.924	<0.001
Abdominal aorta		
PWV	0.81	0.015
VEL_{max}	0.781	0.017
VEL_{avg}	0.71	0.04

ROIs, regions of interest; ICC, intraclass correlation coefficient; TFV, total flow volume; RF, regurgitation fraction; axi-WSS_{max}, maximum axial WSS; axi-WSS_{avg}, average axial WSS; cir-WSS_{max}, maximum circumferential WSS; cir-WSS_{avg}, average circumferential WSS; WSS_{max}, maximum overall wall shear stress; WSS_{avg}, average overall wall shear stress; PWV, pulse wave velocity; VEL_{max}, maximum viscous energy loss; VEL_{avg}, average viscous energy loss.

https://dx.doi.org/10.21037/qims-23-1321

Table S3 Circumferential WSS and axial WSS in 11 ROIs

WSS of 11 ROIs	TAAA (N=11)	AAA (N=19)	Control (N=21)	P value		
				TAAA *vs.* AAA	TAAA *vs.* control	AAA *vs.* control
Ascending aorta (root)						
axi-WSS_{max} (Pa)	1.31 (1.00–1.74)	0.83 (0.60–1.18)	1.06 (0.66–1.80)	0.063	0.483	0.345
axi-WSS_{avg} (Pa)	0.08 (0.07–0.10)	0.07 (0.06–0.08)	0.09 (0.08–0.12)	0.258	0.173	0.003
cir-WSS_{max} (Pa)	1.08 (0.64–1.29)	0.69 (0.59–0.86)	0.87 (0.64–1.47)	0.23	0.885	0.273
cir-WSS_{avg} (Pa)	0.07 (0.06–0.09)	0.07 (0.06–0.08)	0.09 (0.07–0.10)	0.689	0.063	0.028
Ascending aorta (middle)						
axi-WSS_{max} (Pa)	0.81 (0.59–1.39)	1.25 (0.71–1.47)	1.21 (0.70–1.96)	0.29	0.332	0.715
axi-WSS_{avg} (Pa)	0.09 (0.08–0.12)	0.11 (0.10–0.13)	0.13 (0.11–0.15)	0.078	0.01	0.293
cir-WSS_{max} (Pa)	0.54 (0.51–0.88)	0.74 (0.56–1.16)	0.65 (0.49–0.89)	0.466	0.68	0.891
cir-WSS_{avg} (Pa)	0.06 (0.05–0.07)	0.06 (0.06–0.08)	0.08 (0.06–0.08)	0.437	0.027	0.127
Aortic arch at the plane of the brachiocephalic trunk						
axi-WSS_{max} (Pa)	0.58 (0.49–0.96)	0.57 (0.42–0.85)	0.92 (0.56–1.14)	0.854	0.254	0.187
axi-WSS_{avg} (Pa)	0.07 (0.07–0.10)	0.09 (0.07–0.11)	0.11 (0.08–0.14)	0.405	0.009	0.081
cir-WSS_{max} (Pa)	0.31 (0.19–0.57)	0.29 (0.22–0.55)	0.39 (0.24–0.51)	0.902	0.533	0.516
cir-WSS_{avg} (Pa)	0.04 (0.03–0.06)	0.05 (0.04–0.06)	0.06 (0.04–0.08)	0.621	0.058	0.118
Aortic arch at the plane of the left common carotid artery						
axi-WSS_{max} (Pa)	0.76 (0.37–1.11)	0.97 (0.45–1.33)	0.92 (0.46–1.58)	0.46	0.451	0.715
axi-WSS_{avg} (Pa)	0.08 (0.06–0.10)	0.09 (0.07–0.12)	0.11 (0.09–0.14)	0.735	0.093	0.1
cir-WSS_{max} (Pa)	0.64 (0.35–0.81)	0.50 (0.24–0.72)	0.45 (0.25–0.60)	0.622	0.591	0.871
cir-WSS_{avg} (Pa)	0.05 (0.04–0.08)	0.06 (0.05–0.07)	0.07 (0.05–0.09)	0.689	0.575	0.174
Aortic arch at the plane of the left subclavian artery						
axi-WSS_{max} (Pa)	0.56 (0.40–0.84)	0.57 (0.46–0.78)	0.63 (0.48–0.91)	0.815	0.591	0.615
axi-WSS_{avg} (Pa)	0.05 (0.05–0.07)	0.09 (0.06–0.10)	0.09 (0.08–0.10)	0.048	0.003	0.182
cir-WSS_{max} (Pa)	0.34 (0.30–0.57)	0.46 (0.36–0.74)	0.60 (0.38–0.78)	0.204	0.189	0.665
cir-WSS_{avg} (Pa)	0.05 (0.04–0.06)	0.05 (0.04–0.08)	0.09 (0.06–0.10)	0.586	0.011	0.041
Descending aorta at the plane of the pulmonary trunk bifurcation						
axi-WSS_{max} (Pa)	0.61 (0.43–0.91)	1.01 (0.73–1.25)	1.22 (0.93–1.80)	0.036	0.003	0.201
axi-WSS_{avg} (Pa)	0.08 (0.06–0.09)	0.10 (0.09–0.14)	0.14 (0.13–0.22)	0.006	<0.001	0.013
cir-WSS_{max} (Pa)	0.44 (0.26–0.51)	0.50 (0.24–0.76)	0.60 (0.43–0.84)	0.438	0.186	0.377
cir-WSS_{avg} (Pa)	0.04 (0.03–0.07)	0.05 (0.04–0.06)	0.09 (0.07–0.10)	0.54	0.015	0.002

Table S3 (*continued*)

https://dx.doi.org/10.21037/qims-23-1321

Table S3 (*continued*)

WSS of 11 ROIs	TAAA (N=11)	AAA (N=19)	Control (N=21)	P value		
				TAAA *vs.* AAA	TAAA *vs.* control	AAA *vs.* control
Descending aorta at the plane of the heart apex or diaphragm						
axi-WSS_{max} (Pa)	1.01 (0.55–1.53)	1.18 (0.73–1.58)	1.18 (0.97–1.61)	0.466	0.171	0.692
axi-WSS_{avg} (Pa)	0.09 (0.07–0.14)	0.15 (0.12–0.18)	0.18 (0.15–0.23)	0.024	0.002	0.103
cir-WSS_{max} (Pa)	0.41 (0.25–0.92)	0.40 (0.31–0.78)	0.55 (0.25–0.95)	0.832	0.513	0.34
cir-WSS_{avg} (Pa)	0.06 (0.04–0.08)	0.06 (0.04–0.06)	0.07 (0.06–0.08)	0.851	0.131	0.015
Abdominal aorta at the plane of the celiac trunk						
axi-WSS_{max} (Pa)	0.51 (0.44–0.86)	1.05 (0.80–1.24)	1.16 (0.93–2.06)	0.006	0.002	0.185
axi-WSS_{avg} (Pa)	0.08 (0.07–0.11)	0.14 (0.12–0.16)	0.20 (0.17–0.25)	0.002	<0.001	0.002
cir-WSS_{max} (Pa)	0.33 (0.25–0.50)	0.59 (0.30–0.67)	0.52 (0.41–0.83)	0.116	0.065	0.757
cir-WSS_{avg} (Pa)	0.06 (0.04–0.06)	0.07 (0.05–0.07)	0.08 (0.07–0.10)	0.15	0.001	0.023
Abdominal aorta at the plane of the renal artery						
axi-WSS_{max} (Pa)	0.79 (0.40–0.86)	1.16 (0.75–1.36)	1.05 (0.72–1.60)	0.037	0.028	0.989
axi-WSS_{avg} (Pa)	0.08 (0.07–0.10)	0.13 (0.10–0.16)	0.16 (0.13–0.18)	0.01	<0.001	0.05
cir-WSS_{max} (Pa)	0.43 (0.23–0.62)	0.48 (0.32–0.85)	0.37 (0.28–0.78)	0.366	0.451	0.597
cir-WSS_{avg} (Pa)	0.06 (0.04–0.07)	0.05 (0.04–0.09)	0.07 (0.06–0.10)	0.344	0.045	0.218
Abdominal aorta (middle of the abdominal aorta)						
axi-WSS_{max} (Pa)	0.44 (0.28–0.61)	0.59 (0.33–0.73)	1.11 (0.81–1.42)	0.355	<0.001	<0.001
axi-WSS_{avg} (Pa)	0.06 (0.04–0.10)	0.06 (0.05–0.09)	0.17 (0.15–0.20)	0.73	<0.001	<0.001
cir-WSS_{max} (Pa)	0.29 (0.19–0.39)	0.34 (0.25–0.55)	0.55 (0.39–0.87)	0.378	0.023	0.076
cir-WSS_{avg} (Pa)	0.04 (0.03–0.05)	0.04 (0.03–0.05)	0.08 (0.06–0.09)	0.451	<0.001	0.001
Abdominal aorta (aortic bifurcation)						
axi-WSS_{max} (Pa)	0.75 (0.23–0.94)	0.40 (0.27–0.65)	0.85 (0.64–1.10)	0.426	0.226	<0.001
axi-WSS_{avg} (Pa)	0.07 (0.04–0.10)	0.06 (0.05–0.08)	0.12 (0.10–0.16)	0.983	<0.001	<0.001
cir-WSS_{max} (Pa)	0.34 (0.17–0.56)	0.24 (0.18–0.37)	0.47 (0.33–0.61)	0.491	0.204	0.002
cir-WSS_{avg} (Pa)	0.04 (0.03–0.05)	0.04 (0.03–0.04)	0.06 (0.05–0.07)	0.931	0.013	<0.001

All data are given as the median (interquartile range). WSS, wall shear stress; ROIs, regions of interest; TAAA, thoracoabdominal aortic aneurysm; AAA, abdominal aortic aneurysm; axi-WSS_{max}, maximum axial WSS; axi-WSS_{avg}, average axial WSS; cir-WSS_{max}, maximum circumferential WSS; cir-WSS_{avg}, average circumferential WSS.

https://dx.doi.org/10.21037/qims-23-1321